Int. J. Appl. Math. Comput. Sci., 2019, Vol. 29, No. 4, 693–702
DOI: 10.2478/amcs-2019-0051

A TRAJECTORY PLANNING BASED CONTROLLER TO REGULATE AN UNCERTAIN 3D OVERHEAD CRANE SYSTEM

CARLOS AGUILAR-IBANEZ [a,*], MIGUEL S. SUAREZ-CASTANON [b]

[a]Research Center for Computation
National Polytechnic Institute, Av. Juan de Dios Bátiz s/n, UPALM
Col. San Pedro Zacatenco, AP 75476, 07738 Ciudad de México, México
email: carlosaguilari@cic.ipn.mx

[b]Higher School of Computing
National Polytechnic Institute, Av. Juan de Dios Bátiz esq. Av. Miguel Othón de Mendizábal
Col. Lindavista, 07738 Ciudad de México, México
email: sasuarez@prodigy.net.mx

We introduce a control strategy to solve the regulation control problem, from the perspective of trajectory planning, for an uncertain 3D overhead crane. The proposed solution was developed based on an adaptive control approach that takes advantage of the passivity properties found in this kind of systems. We use a trajectory planning approach to preserve the accelerations and velocities inside of realistic ranges, to maintaining the payload movements as close as possible to the origin. To this end, we carefully chose a suitable S-curve based on the Bezier spline, which allows us to efficiently handle the load translation problem, considerably reducing the load oscillations. To perform the convergence analysis, we applied the traditional Lyapunov theory, together with Barbalat's lemma. We assess the effectiveness of our control strategy with convincing numerical simulations.

Keywords: overhead crane, adaptive control, passivity, trajectory planning, Barbalat's lemma.

1. Introduction

Due to the vast range of actual applications, the control of the overhead crane systems has attracted the attention of several researchers in both mechanical engineering and control communities. This heavy machinery has a significant load capacity and high transportation efficiency, and we widely use them, for instances, in building sites, product lines, ports, to transport hazardous materials, and so on. From the theoretical point of view, these cranes belong to underactuated systems and are not input-output linearizable, which make their control a challenging problem. In practice, these cranes are manually operated by experienced workers, having the inconveniences of low efficiency and safety, long time training for operators, and so on (Ramli *et al.*, 2017). We can overcome these inconveniences by providing this kind of cranes with automatic control and secure means, improving their performance and increase the safety of the people who work with and operate them.

In general, overhead crane systems mainly consist of two parallel rails on which a girder slides perpendicularly forwards and backward. There is a cart, mounted on the girder, that moves left and right, and the payload hangs from it using a rope. It is clear that the central control task is bringing the payload from some initial position to another desired final position keeping the oscillations of the suspended payload mass as small as possible. At present, we can find in the literature several techniques to solve the position regulation and the tracking trajectories problems applied to cranes. Due to the kind of tasks that overhead cranes are used for, and despite their nonlinear nature, we can assume that they behave as if they were linear systems because the cart speed is low and the rope angle is small. Additionally, we can easily adapt a Luenberger observer to estimate unavailable velocities.

Consequently, several authors use linearized versions of the crane model when developing control strategies.

*Corresponding author

Therefore, PID and PD based controllers have been widely used in this context. For instance, they have been successfully used when combined with intelligent techniques like neuron networks (Yu *et al*., 2014; Saeidi *et al*., 2013; Suh *et al*., 2005; Hamid *et al*., 2016), fuzzy logic (Smoczek, 2013; Liu *et al*., 2014), particle swarms optimization (Fujioka *et al*., 2015; Hajdu and Gáspár, 2016). Others widely used linear techniques are the ones based on the linear quadratic regulator LQR (Kim *et al*., 2011) and linear matrix inequalities (Sano *et al*., 2011). The LQR method has also been used in conjunction with genetic algorithms (Adeli *et al*., 2011).

On the nonlinear spectra, optimal control based methods have been used, like model predictive control (Wu *et al*., 2015; Jolevski and Bego, 2015; Käpernick and Graichen, 2013; Khatamianfar and Savkin, 2014; Vukov *et al*., 2012; Chen *et al*., 2016; Smoczek and Szpytko, 2017) and the linear quadratic Gaussian predictive approach (Spathopoulos and Fragopoulos, 2004; 2001; Smoczek, 2015). The other well established nonlinear methods that have been applied due to their robustness are adaptive control (Nguyen *et al*., 2015; Cho and Lee, 2008; Fang *et al*., 2012; Sun *et al*., 2014; 2015a; 2015b; 2016; Yang and Shen, 2011; Tar *et al*., 2010; Fujioka and Singhose, 2015a; 2015b; Fujioka *et al*., 2015; Lee *et al*., 2013) and sliding mode control.

Based on a second order sliding mode in conjunction with partial feedback linearization, Kairuz *et al*. (2018) present a robust strategy to solve the regulation problem for a 3D underactuated crane. Results based on the same methodology are presented by Vazquez *et al.* (2012; 2015). Solis *et al*. (2016) use a control strategy for a Cartesian 3D crane based on a terminal optimal control together with an integral sliding mode component (Chwa, 2017) develops a robust finite-time anti-swing tracking control method for a 3D overhead crane system. A full review of this topic is beyond the scope of this study; however, we suggest the interested reader the survey by Ramli *et al*. (2017).

In this work, motivated by the passivity properties found in this kind of systems, and using the adaptive control approach, we developed a control strategy to solve the regulation problem for an underactuated 3D overhead crane. In our solution, we used the trajectory planning approach for two purposes: firstly, to preserve in the actuated coordinate the physical restrictions, like acceleration and velocity, within realistic ranges; secondly, to maintain the payload movements as close as possible to the origin. We made the corresponding convergence analysis applying the traditional Lyapunov theory, together with Barbalat's lemma. To test the effectiveness of our control strategy, we conducted numerical simulations.

We organize the rest of this work as follows. In Section 2, we present the 3D overhead crane dynamic model, and we formulate the control problem we solve in this study. In Section 3, we develop the corresponding control approach. We present the numerical simulations that allow us to assess the effectiveness of our control strategy in Section 4, while we give the concluding remarks in Section 5.

2. Dynamical model and problem statement

The dynamical model of the 3D overhead crane, mentioned above and depicted in Fig. 1, is described in its coordinate form by the following equation:

$$M(\mathbf{q})\ddot{\mathbf{q}} + F_c(\mathbf{q},\dot{\mathbf{q}}) + G(\mathbf{q}) = U - F_d. \qquad (1)$$

The system state is $\mathbf{q} = [x, y, \theta_x, \theta_y]^T$, where x,$y \in \mathbb{R}$ are the cart positions in the horizontal plane and denote its displacement in the x and y axes, respectively. The angular positions of the rope projections in the plane XZ are as follows: θ_x is the swing angle projected onto the XZ-plane, and θ_y is the swing angle measured from the XZ-plane. The system inertia matrix $M(\cdot)$ is defined as:[1]

$$M(\mathbf{q}) = \begin{bmatrix} M_x + m & 0 & lmC_xC_y & -lmS_xS_y \\ 0 & M_y + m & 0 & lmC_y \\ lmC_xC_y & 0 & l^2mC_y^2 & 0 \\ -lmS_xS_y & lmC_y & 0 & l^2m \end{bmatrix},$$

where $F_c(\cdot)$ is referred to as the centripetal-Coriolis vector force, and is defined as

$$F_c(\mathbf{q},\dot{\mathbf{q}}) = \begin{bmatrix} -lmC_yS_x\dot{\theta}_x^2 - 2lmC_xS_y\dot{\theta}_x\dot{\theta}_y - lmC_yS_x\dot{\theta}_y^2 \\ -lmS_y\dot{\theta}_y^2 \\ -2l^2mS_yC_y\dot{\theta}_x\dot{\theta}_y \\ l^2mS_yC_y\dot{\theta}_x^2 \end{bmatrix}.$$

The gravity force effect, denoted by $G(\cdot)$, is expressed as

$$G(\mathbf{q}) = \begin{bmatrix} 0 & 0 & mglS_xC_y & mglC_xS_y \end{bmatrix}^T.$$

Finally, the control input vector U and the dissipative force F_d are given by

$$U = \begin{bmatrix} f_x & f_y & 0 & 0 \end{bmatrix}^T,$$

$$F_d = \big[d_x\dot{x} + f_{cx}(\dot{x}) \quad d_y\dot{x} + f_{cy}(\dot{y}) \quad d_{\theta_x}\dot{\theta}_x \quad d_{\theta_y}\dot{\theta}_y\big]^T,$$

[1] We use the notation $C_\theta = \cos\theta$ and $S_\theta = \cos\theta$, with $\theta = \{\theta_x, \theta_y\}$.

where f_x is the driving force of x motion, and f_y is that of y motion. The constant system parameters M_x and M_y are respectively the components in directions x and y of the crane mass and the equivalent masses of the rotating parts, i.e., motors and their drive trains; m is the load mass, g is the gravitational acceleration, l is the rope length. d_x, d_y, d_{θ_x}, and d_{θ_x} denote the viscous damping coefficients related with x, y, θ_x and θ_y motions, respectively. Finally, $f_{cx}(\dot{x})$ and $f_{cy}(\dot{y})$ are the Coulomb friction forces approximated by the following continuous function:

$$f_{cw}(\dot{w}) = \frac{-\beta_w \dot{w}}{\sqrt{\dot{w}^2 + \alpha}}, \quad \beta_w > 0, \alpha > 0, \quad \alpha \to 0 \quad (2)$$

with $w = \{x, y\}$ (cf. Gómez-Estern *et al*., 2004).

Remark 1. The rope from which the loads hangs from the crane is a massless and rigid link, with positive and constant length l. During the transportation process, the swing angles of the load always remain in the interval θ_x, $\theta_y \in I = (-\pi, \pi)$. That is, for simplicity, we are not considering the dynamic in the direction of l. We chose the Coulomb friction forces as an approximation to avoid control discontinuities and the chattering phenomena. Additionally, we pointed out that it is easy to see that system (1) has a subset of stable equilibrium points, if $\mathbf{q} = [x = *, y = *, \theta_x = 0, \theta_y = 0]^T$.

Motivation. In this work, we solve the regulation problem for an uncertain damped overhead crane system, based on a trajectory planning strategy through the actuated coordinate. *The main advantage of our solution consists in maintaining the payload oscillations as close as possible to the origin, which is an attractive problem due to their actual applications. Additionally, the solution that we propose allows us to set* a priori *the load translation task duration.* To this end, we use as a trajectory reference a *Bézier* function, which is, in fact, an off-line planning motion. Using this reference, allows us to program the admissible convergence period of time, and keep the linear velocities ($\dot{x}$,$\dot{y}$) and the accelerations ($\ddot{x}$,$\ddot{y}$) within an admissible set, and the oscillations of θ_x and θ_y within a small vicinity of the origin. It is important to mention that the *Bézier* function used, can be seen as a particular case of the S-curves to solve the overhead crane motion planning used by Fang *et al*. (2012) and Lee (2005).

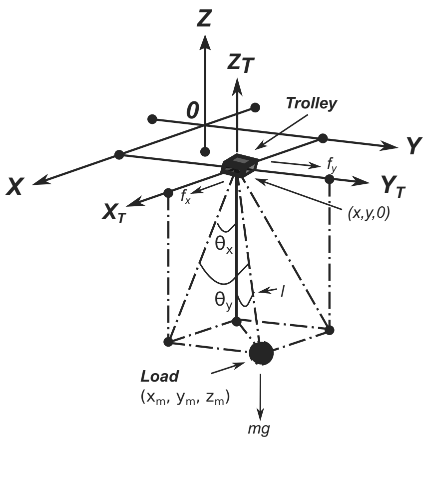

Fig. 1. Overhead crane.

Having described the model of the 3D overhead crane, we proceed to establish the control goal of this study.

Control problem. *Consider the task of translating the payload of a 3D overhead crane from some initial position*[2]

$$q_i = (x_i, y_i, \theta_x, \theta_y)^T$$

to a desired final rest final position

$$q_f = (x_f, y_f, 0, 0)^T$$

in some time interval $[t_i, t_f]$, *with* $t_f > t_i \geq 0$, *preserving the following physical restrictions:*

$$\begin{aligned} \left|\dot{x}(t)\right| &< z_v, \quad \left|\ddot{x}(t)\right| < z_a, \\ \left|\dot{y}(t_i)\right| &< z_v, \quad \left|\ddot{y}(t)\right| < z_a \end{aligned}$$

for all $t \in [0, \infty)$, *where constants* z_i, *with* $i = \{v, a\}$, *are known. The control objective consists in accomplishing the above translation task in a given finite time interval* $[t_i, t_f]$, *such that the payload swinging remains close enough to zero, even when the physical system parameters are unknown. Formally, we desire that*

$$\begin{aligned} |x(t) - x_f| &\leq \delta_1, \qquad & |y(t) - y_f| &\leq \delta_1, \\ |\theta_x(t)| &\leq \delta_2, \qquad & |\theta_y(t)| &\leq \delta_2, \end{aligned}$$

for $t \in [t_i, t_f]$ *and* $\lim_{t\to\infty} q(t) = q_f$, *with* δ_1 *and* δ_2 *sufficiently small. The above is to be solved on the following assumptions: (i) the whole state is always available; (ii)* θ_x, $\theta_y \in I = (-\pi, \pi)$; *and (iii) all the unknown damping coefficients are strictly positive, and the physical parameters are unknown.*

Assumptions and limitations. We assume that the position (x, y) and its corresponding velocities are available. Additionally, the controller does not have any information about the physical parameters of the 3D crane. On the other hand, in our solution, the velocity needs to be included in feedback, which in actual applications is not available, and has to be estimated using a suitable observation scheme. Besides, our solution is not immune to external perturbations and unmodeled dynamics; however, it can be overcome using an extended

[2]For simplicity, we write $z_i = z(t_i)$ and $z_f = z(t_f)$.

observer, like the ones used in active disturbance rejection control (Zheng and Gao, 2010; Huang *et al.*, 2014), or a convenient slide mode based method (Davila *et al.*, 2006; Ferreira *et al.*, 2010).

Some useful properties of the Euler–Lagrange systems.
A1: $M(\mathbf{q})$ is a symmetric and positive definite matrix.
A2: The centripetal-Coriolis vector force admits the following representation:

$$F_c(\mathbf{q}, \dot{\mathbf{q}}) = C(\mathbf{q}, \dot{\mathbf{q}})\dot{\mathbf{q}},$$

where C satisfies the following condition:

$$\dot{M}(\mathbf{q}) - 2C(\mathbf{q}, \dot{\mathbf{q}}) = -(\dot{M}(\mathbf{q}) - 2C(\mathbf{q}, \dot{\mathbf{q}}))^T.$$

A3: The vector $G(\mathbf{q})$ is a gradient. That is,

$$G(\mathbf{q}) = \frac{\partial P(\mathbf{q})}{\partial \mathbf{q}},$$

where $P(\mathbf{q}) = mgl\,(1 - C_x C_y)$.
A4: Given the energy function

$$E(\mathbf{q}, \dot{\mathbf{q}}) = \frac{1}{2}\dot{\mathbf{q}}^T M(\mathbf{q})\dot{\mathbf{q}} + P(\mathbf{q}),$$

if $F_d = 0$, we have that

$$\dot{E}(\mathbf{q}, \dot{\mathbf{q}}) = \dot{x} f_x + \dot{y} f_y.$$

This implies

$$\int_0^t (\dot{x} f_x + \dot{y} f_y)\,\mathrm{d}s \geq -E(0).$$

That is, if $f = (f_x, f_y)$ and $y = (\dot{x}, \dot{y})$ are, respectively, the input and output of the system, then it is a passive system (a complete treatment of the properties of the Euler–Lagrange systems can be found in the work of Ortega *et al.* (2013)).

Trajectory planning. In order to solve the control problem, we propose the convenient trajectories, referred here as $x_d(t)$ and $y_d(t)$, in the form

$$\begin{aligned} x_d(t) &= x_i + (x_f - x_i)\lambda(t, t_i, t_f), \\ y_d(t) &= y_i + (y_f - y_i)\lambda(t, t_i, t_f), \end{aligned} \tag{3}$$

where $\lambda(t, t_i, t_f)$ is a *Bézier* spline (Sira-Ramirez and Agrawal, 2004) defined as

$$\lambda(t, t_i, t_f) = \begin{cases} 0 & \text{if} \quad t < t_i, \\ \Delta(t) \sum\limits_{i=1}^{6} (-1)^{i+1} r_i \Delta^{i-1}(t) & \text{if} \quad t_i \leq t \leq t_f, \\ 1 & \text{if} \quad t > t_f, \end{cases} \tag{4}$$

where

$$\begin{aligned} r_1 &= 252, & r_2 &= 1050, & r_3 &= 1800, \\ r_4 &= 1575, & r_5 &= 700, & r_6 &= 126, \end{aligned}$$

$\Delta(t) = (t - t_i)/\delta_T$, with $\delta_T = t_f - t_i$. It is easy to check that this polynomial satisfies the following properties:
B1:

$$\begin{aligned} \left.\frac{\mathrm{d}^k}{\mathrm{d}t^k}\lambda(t, t_i, t_f)\right|_{t=t_i} &= 0, \\ \left.\frac{\mathrm{d}^k}{\mathrm{d}t^k}\lambda(t, t_i, t_f)\right|_{t=t_f} &= 0 \end{aligned} \tag{5}$$

for $k = \{0, 1, \dots, n\}$.
B2:

$$\begin{aligned} \dot{\lambda}(t, t_i, t_f) &< \frac{\kappa_1}{\delta_T} = \frac{2.61}{t_f - t_i}, \\ \ddot{\lambda}(t, t_i, t_f) &< \frac{\kappa_2}{\delta_T^2} = \frac{11.01}{(t_f - t_i)^2}. \end{aligned} \tag{6}$$

B3: $\dot{\lambda}(t, t_i, t_f) \in L_2^2$ and $\ddot{\lambda}(t, t_i, t_f) \in L_2^2$. Hence, $\dot{x}_d(t)$, $\dot{y}_d(t) \in L_2^2$ and $\ddot{x}_d(t)$, $\ddot{y}_d(t) \in L_2^2$.

Finally, we say that $x_d(t)$ and $y_d(t)$ are admissible trajectories if they satisfy the following inequalities:

$$\begin{aligned} \max\left\{\frac{\kappa_1}{\delta_T}(x_f - x_i), \frac{\kappa_1}{\delta_T}(y_f - y_i)\right\} &< z_v, \\ \max\left\{\frac{\kappa_2}{\delta_T^2}(x_f - x_i), \frac{\kappa_2}{\delta_T^2}(y_f - y_i)\right\} &< z_a. \end{aligned} \tag{7}$$

For a proof of these properties, see Appendix.

3. Control strategy

In this section, we derive a passivity-based controller, in conjunction with an adaptive compensator to solve the trajectories planning problem of a three-dimensional overhead crane. To achieve this, we first propose the following nonnegative energy function:

$$E(\overline{\mathbf{q}}, \dot{\overline{\mathbf{q}}}) = \frac{1}{2}\dot{\overline{\mathbf{q}}}^T M(\mathbf{q})\dot{\overline{\mathbf{q}}} + mgl(1 - \cos\theta_x \cos\theta_y), \tag{8}$$

where

$$\begin{aligned} \overline{\mathbf{q}} &= [r_x, r_y, \theta_x, \theta_y]^T, \\ r_x &= x - x_d, \\ r_y &= y - y_d. \end{aligned} \tag{9}$$

Taking the time derivative of A2 along the trajectories of (1) is easy to show, using properties B2 and b3, that the following equality holds:

$$\dot{E} = \dot{r}_x(f_x - f_{d_x}) + \dot{r}_y(f_y - f_{d_y}) + W_0 + W_1, \tag{10}$$

where

$$\begin{aligned} f_{d_x} &= d_x\dot{x} + f_{cx}(\dot{x}) + (M_x+m)\ddot{x}_d,\\ f_{d_y} &= d_x\dot{y} + f_{cy}(\dot{y}) + (M_y+m)\ddot{y}_d,\\ W_0 &= -d_{\theta_x}\dot{\theta}_x^2 - d_{\theta_y}\dot{\theta}_y^2,\\ W_1 &= -lmC_xC_y\dot{\theta}_x\ddot{x}_d + lmS_xS_y\dot{\theta}_y\ddot{x}_d\\ &\quad - lmC_y\dot{\theta}_y\ddot{y}_d. \end{aligned} \tag{11}$$

As all the system parameters are unknown, except for the parameter α associated with approximation functions of the Coulomb friction force (see (2)), we can express f_{d_x} and f_{d_y} as follows:

$$f_{d_x} = \Phi_x^T(t)\varpi_x, \quad f_{d_y} = \Phi_y^T(t)\varpi_y,$$

where

$$\begin{aligned} \varpi_x &= \begin{bmatrix} d_x & \beta_x & M_x+m \end{bmatrix}^T,\\ \Phi_x(t) &= \begin{bmatrix} \dot{x} & \dfrac{\dot{x}}{\sqrt{\dot{x}^2+\alpha}} & \ddot{x}_d(t) \end{bmatrix}^T,\\ \varpi_y &= \begin{bmatrix} d_y & \beta_y & M_y+m \end{bmatrix}^T,\\ \Phi_y(t) &= \begin{bmatrix} \dot{y} & \dfrac{\dot{y}}{\sqrt{\dot{y}^2+\alpha}} & \ddot{y}_d(t) \end{bmatrix}^T. \end{aligned} \tag{12}$$

Therefore, we propose the adaptive tracking controller as

$$f_x = -k_pr_x - k_d\dot{r}_x - \Phi_x^T(t)\widehat{\varpi}_x, \tag{13}$$

$$f_y = -k_pr_y - k_d\dot{r}_y - \Phi_y^T(t)\widehat{\varpi}_y, \tag{14}$$

where k_p and k_d are positive control gains; $\widehat{\varpi}_x$ and $\widehat{\varpi}_y$ are, respectively, the online estimates of ϖ_x and ϖ_y, which evolve according to the following adaptive laws:

$$\dot{\widehat{\varpi}}_x = \Gamma\Phi_x(t)r_x, \tag{15}$$

$$\dot{\widehat{\varpi}}_y = \Gamma\Phi_y(t)r_y \tag{16}$$

with Γ being a diagonal, positive definite, update gain matrix.

3.1. Stability analysis.

Once we designed the control law, we propose the required Lyapunov function to make stability analysis assure convergence. To this end, we introduce the main result of this study.

Proposition 1. *Consider the system (1), in closed-loop with (13) and (14), and the admissible trajectories x_d and y_d, both defined in (3). Then the closed-loop system asymptotically converges fast to a neighborhood of zero and $\lim_{t\to\infty}\overline{\mathbf{q}}(t)=0$, with the computable domain of attraction given by $V(0) < 2mgl$, with V defined below.*

Proof. For simplicity, we assume that $d_\theta = d_{\theta_x} = d_{\theta_y} > 0$. Now, consider the following candidate Lyapunov function:

$$\begin{aligned} V(t) &= E(\overline{\mathbf{q}},\dot{\overline{\mathbf{q}}}) + \frac{k_p}{2}\left(r_x^2+r_y^2\right) + \frac{1}{2}\left(\dot{r}_x^2+\dot{r}_y^2\right)\\ &\quad + \frac{1}{2}\left(\widetilde{\varpi}_x^T\Gamma^{-1}\widetilde{\varpi}_x + \widetilde{\varpi}_y^T\Gamma^{-1}\widetilde{\varpi}_y\right), \end{aligned} \tag{17}$$

where $\widetilde{\varpi}_x = \varpi_x - \widehat{\varpi}_x$ and $\widetilde{\varpi}_y = \varpi_y - \widehat{\varpi}_y$. Computing the time derivative of (17) and using (10) and the formulas (13)–(16), is easy to see that

$$\dot{V}(t) = -k_d(\dot{r}_x^2+\dot{r}_y^2) + W_0 + W_1, \tag{18}$$

where W_0 and W_1 were previously defined in (11). On the other hand, we can note that W_1 can be upper bounded by the following inequality:

$$W_1 \le \frac{lm}{2\gamma}\dot{\theta}_x^2 + \frac{\gamma lm}{2}\ddot{x}_d^2 + \frac{lm}{2\gamma}\dot{\theta}_y^2 + \frac{\gamma lm}{2}\ddot{x}_d^2 + \frac{lm}{\gamma}\ddot{y}_d^2,$$

where $\gamma > 0$. Hence, selecting γ, such that

$$-d_\theta + lm/2\gamma > -\varepsilon,$$

with $\varepsilon > 0$, is easy to see that

$$W_0 + W_1 \le -\varepsilon\big(\dot{\theta}_x^2 + \dot{\theta}_y^2\big) + \frac{\gamma lm}{2}\ddot{x}_d^2 + \frac{lm}{\gamma}\ddot{y}_d^2. \tag{19}$$

Substituting (19) into (18), we obtain

$$\begin{aligned} \dot{V}(t) &\le -k_d(\dot{r}_x^2+\dot{r}_y^2) - \varepsilon\big(\dot{\theta}_x^2 + \dot{\theta}_y^2\big)\\ &\quad + \frac{\gamma lm}{2}\ddot{x}_d^2 + \frac{lm}{\gamma}\ddot{y}_d^2. \end{aligned} \tag{20}$$

Now, integrating both the sides of (20), we have

$$\begin{aligned} k_d\textstyle\int_0^T(\dot{r}_x^2+\dot{r}_y^2) + \varepsilon\int_0^T\big(\dot{\theta}_x^2+\dot{\theta}_y^2\big) + V(T)&\\ \le V(0) + \frac{\gamma lm}{2}\textstyle\int_0^T\ddot{x}_d^2 + \frac{lm}{\gamma}\int_0^T\ddot{y}_d^2.& \end{aligned} \tag{21}$$

Since $\ddot{x}_d(t), \ddot{y}_d(t) \in L_2$,

$$V(T) \le V(0) + \frac{\gamma lm}{2}\int_0^T\ddot{x}_d^2 + \frac{lm}{\gamma}\int_0^T\ddot{y}_d^2 < \overline{V} < \infty.$$

Consequently, $V(T) \in L_\infty$ and the set of signals:

$$\Big\{\overline{\mathbf{q}}, \dot{\overline{\mathbf{q}}}, r_x, r_y, \dot{r}_x, \dot{r}_y, \widetilde{\varpi}_x, \widetilde{\varpi}_y\Big\} \in L_\infty. \tag{22}$$

Notice that if the above conditions are fulfilled, then the following conditions are also fulfilled:

$$\big\{\mathbf{q}, \dot{\mathbf{q}}, x, y, \dot{x}, \dot{y}, \widehat{\varpi}_x, \widehat{\varpi}_y\big\} \in L_\infty.$$

From the definitions of $\overline{\mathbf{q}}$ and $\dot{\overline{\mathbf{q}}}$, both given in (9), we have that $(\mathbf{q},\dot{\mathbf{q}}) \in L_\infty$. Therefore, according to the definitions of $\Phi_x(t)$ and $\Phi_y(t)$, both given in (12), we conclude that $(\Phi_x(t), \Phi_y(t)) \in L_\infty$, implying that f_x and f_y also belong to L_∞ (see (13) and (14)). These facts and Eqn. (1), allow us to conclude that $(\ddot{\mathbf{q}}, \ddot{\overline{\mathbf{q}}}) \in L_\infty$. Consequently, $(\ddot{r}_x, \ddot{r}_y) \in L_\infty$. Summarizing,

$$\{\ddot{x}, \ddot{y}, \ddot{\theta}_x, \ddot{\theta}_y, \ddot{r}_x, \ddot{r}_y\} \in L_\infty. \tag{23}$$

From the inequality (21), we have

$$k_d \int_0^T (\dot{r}_x^2 + \dot{r}_y^2) + \varepsilon \int_0^T \left(\dot{\theta}_x^2 + \dot{\theta}_y^2\right) \le \overline{V},$$

which implies that $\{\dot{\theta}_x, \dot{\theta}_y, \dot{r}_x, \dot{r}_y\} \in L_2^2$. Now, as $\{\dot{\theta}_x, \dot{\theta}_y, \dot{r}_x, \dot{r}_y\} \in L_2 \cap L_\infty$ and $\{\ddot{\theta}_x, \ddot{\theta}_y, \ddot{r}_x, \ddot{r}_y\} \in L_\infty$, then, according to Barbalat's lemma (Khalil, 2015), we have that

$$\begin{aligned} &\lim_{t\to\infty} \dot{\theta}_x(t) = 0, \quad \lim_{t\to\infty} \dot{\theta}_y(t) = 0, \\ &\lim_{t\to\infty} \dot{r}_x(t) = 0, \quad \lim_{t\to\infty} \dot{r}_y(t) = 0. \end{aligned} \tag{24}$$

From the facts above and the definition of $\dot{r}_x = \dot{x} - x_d$ and $\dot{r}_y = \dot{y} - y_d$, we conclude that $\dot{x}$ and $\dot{y}$ converge asymptotically to zero. Hence, $\Phi_x(t)$,$\Phi_y(t) \to 0$, as long as $t \to \infty$, implying that $\Phi_x^T(t)\widehat{\varpi}_x$,$\Phi_y^T(t)\widehat{\varpi}_y \to 0$. Therefore, using the definitions of f_x and f_y, respectively given in (13) and (14), it is clear that

$$\lim_{t\to\infty} f_x = -k_p \lim_{t\to\infty} r_x, \qquad \lim_{t\to\infty} f_y = -k_p \lim_{t\to\infty} r_y. \tag{25}$$

Now, as the set of signals $\{\dot{x}, \dot{y}, \dot{\theta}_x, \dot{\theta}_y\}$ is well defined, and $\{\ddot{x}, \ddot{y}, \ddot{\theta}_x, \ddot{\theta}_y\} \in L_\infty$, once again applying Barbalat's lemma, we have that

$$\begin{aligned} &\lim_{t\to\infty} \ddot{\theta}_x(t) = 0, \qquad \lim_{t\to\infty} \ddot{\theta}_y(t) = 0, \\ &\lim_{t\to\infty} \ddot{x}(t) = 0. \qquad \lim_{t\to\infty} \ddot{y}(t) = 0. \end{aligned} \tag{26}$$

Based on (24)–(3.1), is easy to see that Eqn. (1) leads to

$$\begin{aligned} \Big[-k_p \lim_{t\to\infty} r_x \quad -k_p \lim_{t\to\infty} r_x \quad -mgl \lim_{t\to\infty} S_x C_y \\ -mgl \lim_{t\to\infty} C_x S_y\Big] = 0. \end{aligned}$$

Because we assume that $(\theta_x, \theta_y) \in (-\pi/2, \pi/2)$, we conclude that $\{x \to x_d,\ y \to y_d, \theta_x \to 0, \theta_y \to 0\}$. Notice that the assumption $(\theta_x, \theta_y) \in (-\pi/2, \pi/2)$ can be assured if the set of initial conditions satisfies

$$V(0) < mgl.$$

■

4. Numerical simulations

In order to test the effectiveness of our control strategy, we designed two hypothetical numerical experiments:

First experiment. The task consists in translating the payload from the initial position given as $q_i = [0.1\,\text{m}, 0.1\,\text{m}, 0.2\,\text{rad}, -0.15\,\text{rad}]$ with $p_i = 0$, to the final rest position $q_f = [1\,\text{m}, 1.1\,\text{m}, 0, 0]$ with $p_f = 0$, within the time interval $[t_i, t_f] = [0, 10\,\text{s}]$, and an integration step of order $h = 10^{-4}$. For the set-up, we fixed the constant physical parameters as follows:

$$\begin{aligned} &M_x = 90\,\text{kg}, && M_y = 100\,\text{kg}, && m = 50\,\text{kg}, \\ &l = 1\,\text{m}, && d_x = 0.5, && d_y = 0.5, \\ &d_{\theta_x} = 0.2, && d_{\theta_y} = 0.15, && \beta_{wx} = 0.3, \\ &\beta_{wy} = 0.25, && z_v = 1\,\text{m/s}, && z_a = 0.5\,\text{m/s}^2, \end{aligned}$$

with $\alpha = 5 \times 10^{-3}$. We fixed the control gains as $k_p = 50$ and $k_d = 53$; the matrix $\Gamma = \text{diag}(1, 1, 2, 2)$. Additionally, in this experiment, we made a behavior comparison between our control strategy (OCS) and the traditionally PD-based controller (PD), where the trajectory planning for PD was not included. We presented the obtained results in Fig. 2, where we can see that OCS accomplishes the control task satisfactorily within the programmed time interval.

It is worth of mentioning that, after 10 seconds, positions x and y almost reach the desired rest position, and angles θ_x and θ_y converge in the small vicinity of ± 0.04 rad; conversely, the closed-loop response of the traditional PD remains oscillating after 10 s. That is, the position variables have an average error of ± 0.12 m, while the error of the angular variable θ_x and θ_y is on the average ± 0.1rad. From the comparison, we can see that OCS outperforms the traditional PD. We show the system velocities in Fig. 3. As we can see in this figure, the velocity closed-loop responses of OCS are very close to zero, that is $|p| \approx 10^{-3}$, while the corresponding velocities for the closed-loop of PD are almost $|p| \approx 0.1$. Once again, from this figure, we can claim that OCS has a much better performance than the PD controller. Finally, we show the corresponding control action behavior in Fig. 4, where we can see that OCS is ranging in $|f_x| \approx 0.01\,\text{Nw}$ and $|f_y| \approx 0.05\,\text{Nw}$, while the PD is ranging in $|f_x| \approx 0.5\,\text{Nw}$ and $|f_y| \approx 1$ Nw. We pointed out that the OCS closed-loop response is able to follow admissible trajectories, as we formally established in (7). On the other hand, it is easy to see in the figures that the PD closed-loop response exhibits an abrupt behavior in comparison with OCS.

Second experiment. Here we carry out a numerical comparison between our control strategy and a first-order slide-mode control strategy (SMS), based on the approaches found in the work of Qian and Yi (2016) or

Sira-Ramirez and Agrawal (2004). To this end, we use the same parameters set up as in the previous simulation, except that we take the following physical parameters values from the work of Kairuz *et al.* (2018): $M_x = 3.3$ kg, $M_y = 1.5$ kg, $m = 1\,\mathrm{kg}$, and $l = 0.6\,\mathrm{m}$. To make the experiment more interesting and challenging, we add the following perturbation in the actuated coordinates: $\delta_x = 0.2\sin(3t)\cos(2t)$ and $\delta_y = 0.25\sin(3t)\cos(5t)$.

To implement the first-order slide-mode controller, we select the following two sliding surfaces:

$$\sigma_x = (z_1 - \kappa x_f) + 3z_2 + 3z_3 + z_4,$$
$$\sigma_y = (w_1 - \kappa y_f) + 3w_2 + 3w_3 + w_4,$$

where

$$z_1 = \theta_x + \kappa x, \qquad z_2 = \dot{\theta}_x + \kappa \dot{x},$$
$$z_3 = -\frac{g}{l}\theta_x, \qquad z_3 = -\frac{g}{l}\dot{\theta}_x,$$
$$w_1 = \theta_y + \kappa y, \qquad w_2 = \dot{\theta}_y + \kappa \dot{y},$$
$$w_3 = -\frac{g}{l}\theta_y, \qquad w_4 = -\frac{g}{l}\dot{\theta}_y,$$

with $\kappa = 1/l$. In our case, f_x and f_y are proposed, such that

$$\dot{\sigma}_x = -\mathrm{sign}(\sigma_x), \quad \sigma_y = -\mathrm{sign}(\sigma_y).$$

We show the outcomes of this simulation in Fig. 5, where we can see the evolution of coordinates x and y, with their corresponding angles. As we expected, the SMS behavior outperforms OCS. However, SMS exhibits the undesirable chattering phenomena and needs more information about the system structure and the knowledge of the values of the parameters. In favor of OCS, we can say that it solves the regulation problem in a practical manner because the angles oscillate close to the origin due to the presence of non-vanishing external perturbations. Also, in this figure, we can see the control behavior of both controllers, where once again it becomes evident the presence of both chattering phenomena in SMS and the nonvanishing perturbations in OCS.

Remark 2. Our control approach was designed taking advantage of the passivity property found in the kind of mechanical systems that we are dealing with. Therefore, our controller is simple, and it only uses the positions and their corresponding velocities. Even more, due to its nature, our approach does not use any angular information, unlike other control laws based on sliding modes, which need information about the angular variables and the knowledge of the physical parameters (Qian and Yi, 2016; Kairuz *et al.*, 2018). In the light of these facts, our approach is less efficient and less robust against external perturbations and unmodeled dynamics, than the ones based on sliding modes. However, the latter exhibit the chattering phenomena and need more information than our approach.

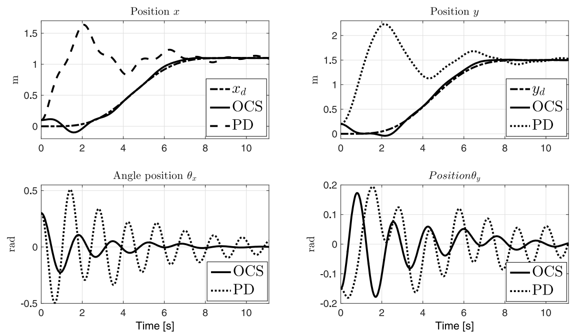

Fig. 2. Comparison of the closed-loop response positions between OCS and a traditional PD.

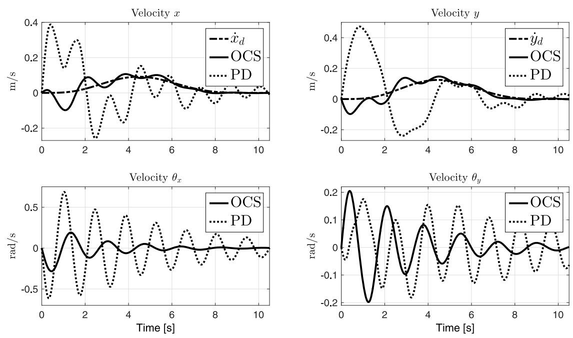

Fig. 3. Comparison of the closed-loop response velocities between OCS and a traditional PD.

5. Conclusions

Based on trajectory planning, we have solved the regulation problem for an uncertain 3D overhead crane. To program the reference trajectory, we use a *Bézier* function. This function can be considered as a particular case of S-curves, which have been widely suggested by the control community to solve the trajectory motion planning problem due to some suitable properties. We designed the control strategy taking advantage of the passivity properties found in the kind of crane systems we are dealing with, together with the traditional adaptive control approach.

Off-line trajectory planning has two purposes. First, it allows us to program the admissible period of time, in which the control task has to be accomplished, preserving the realistic physical restrictions in the linear velocities and accelerations, while the payload angles always remain inside of a small vicinity of the origin. Intuitively, this means that the longer the translation time, the smaller the payload oscillation angles. We made the corresponding convergence analysis applying the traditional Lyapunov theory, together with Barbalat's lemma. To test the effectiveness of our control strategy, we conducted

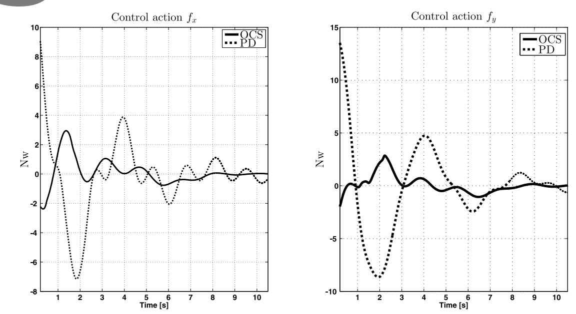

Fig. 4. Comparison between the control actions of OCS and a traditional PD.

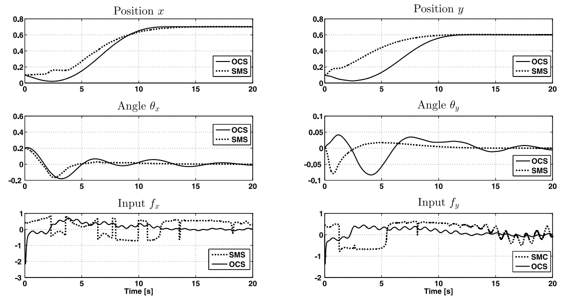

Fig. 5. Comparison between the control actions of OCS and SMS.

numerical simulations. We finish mentioning that our control scheme could be improved if an extended high-order observer were added to actively reject bounded unknown perturbations, as it is done in ADRC.

Acknowledgment

The original name of C. Aguilar-Ibanez's affiliation is Centro de Investigacion en Computacion, Instituto Politecnico Nacional, while that of M.S. Suarez-Castanon's is Escuela Superior de Computo, Instituto Politecnico Nacional.

References

Adeli, M., Zarabadipour, H., Zarabadi, S.H. and Shoorehdeli, M.A. (2011). Anti-swing control for a double-pendulum-type overhead crane via parallel distributed fuzzy LQR controller combined with genetic fuzzy rule set selection, *IEEE International Conference on Control System, Computing and Engineering (ICCSCE), Penang, Malaysia,* pp. 306–311.

Chen, H., Fang, Y. and Sun, N. (2016). A swing constraint guaranteed MPC algorithm for underactuated overhead cranes, *IEEE/ASME Transactions on Mechatronics* **21**(5): 2543–2555.

Cho, H.C. and Lee, K.S. (2008). Adaptive control and stability analysis of nonlinear crane systems with perturbation, *Journal of Mechanical Science and Technology* **22**(6): 1091.

Chwa, D. (2017). Sliding-mode-control-based robust finite-time antisway tracking control of 3-D overhead cranes, *IEEE Transactions on Industrial Electronics* **64**(8): 6775–6784.

Davila, J., Fridman, L. and Poznyak, A. (2006). Observation and identification of mechanical systems via second order sliding modes, *International Journal of Control* **79**(10): 1251–1262.

Fang, Y., Ma, B., Wang, P. and Zhang, X. (2012). A motion planning-based adaptive control method for an underactuated crane system, *IEEE Transactions on Control Systems Technology* **20**(1): 241–248.

Ferreira, A., Bejarano, F.J. and Fridman, L.M. (2010). Robust control with exact uncertainties compensation: With or without chattering?, *IEEE Transactions on Control Systems Technology* **19**(5): 969–975.

Fujioka, D., Shah, M. and Singhose, W. (2015). Robustness analysis of input-shaped model reference control on a double-pendulum crane, *American Control Conference (ACC), Chicago, IL, USA*, pp. 2561–2566.

Fujioka, D. and Singhose, W. (2015a). Input-shaped model reference control of a nonlinear time-varying double-pendulum crane, *10th Asian Control Conference (ASCC), Kota Kinabalu, Malaysia*, pp. 1–6.

Fujioka, D. and Singhose, W. (2015b). Performance comparison of input-shaped model reference control on an uncertain flexible system, *IFAC-PapersOnLine* **48**(12): 129–134.

Gómez-Estern, F., Van der Schaft, A. and Acosta, J. (2004). Passivation of underactuated systems with physical damping, *6th IFAC Symposium on Nonlinear Control Systems, Stuttgart, Germany*, pp. 1–3.

Hajdu, S. and Gáspár, P. (2016). Reducing the mast vibration of single-mast stacker cranes by gain-scheduled control, *International Journal of Applied Mathematics and Computer Science* **26**(4): 791–802, DOI: 10.1515/amcs-2016-0056.

Hamid, M., Jamil, M., Gilani, S.O., Ikramullah, S., Khan, M.N., Malik, M.H. and Ahmad, I. (2016). Jib system control of industrial robotic three degree of freedom crane using a hybrid controller, *Indian Journal of Science and Technology* **9**(21).

Huang, Y., Xue, W., Zhiqiang, G., Sira-Ramirez, H., Wu, D. and Sun, M. (2014). Active disturbance rejection control: Methodology, practice and analysis, *33rd Chinese Control Conference, Nanjing, China*, pp. 1–5.

Jolevski, D. and Bego, O. (2015). Model predictive control of gantry/bridge crane with anti-sway algorithm, *Journal of Mechanical Science and Technology* **29**(2): 827–834.

Kairuz, R.I.V., Aguilar, L.T., de Loza, A.F. and Garcia, J.E.A. (2018). Robust positioning control law for a 3d underactuated crane system, *IFAC-PapersOnLine* **51**(13): 450–455.

Käpernick, B. and Graichen, K. (2013). Model predictive control of an overhead crane using constraint substitution, *2013 American Control Conference, Washington, DC, USA*, pp. 3973–3978.

Khalil, H.K. (2015). *Nonlinear Control*, Pearson, New York, NY.

Khatamianfar, A. and Savkin, A.V. (2014). A new tracking control approach for 3D overhead crane systems using model predictive control, *European Control Conference (ECC), Strasbourg, France*, pp. 796–801.

Kim, D., Park, Y., Park, Y.-s., Kwon, S. and Kim, E. (2011). Dual stage trolley control system for anti-swing control of mobile harbor crane, *11th International Conference on Control, Automation and Systems, Gyeonggi-do, Korea*, pp. 420–423.

Lee, H.-H. (2005). Motion planning for three-dimensional overhead cranes with high-speed load hoisting, *International Journal of Control* **78**(12): 875–886.

Lee, S.-G., Nho, L.C. and Kim, D.H. (2013). Model reference adaptive sliding mode control for three dimensional overhead cranes, *International Journal of Precision Engineering and Manufacturing* **14**(8): 1329–1338.

Liu, C., Zhao, H. and Cui, Y. (2014). Research on application of fuzzy adaptive PID controller in bridge crane control system, *5th IEEE International Conference on Software Engineering and Service Science (ICSESS), Beijing, China,* pp. 971–974.

Nguyen, Q.C., Ngo, H.-Q.T. and Kim, W.-H. (2015). Nonlinear adaptive control of a 3d overhead crane, *15th International Conference on Control, Automation and Systems (ICCAS), Busan, Korea,* pp. 41–47.

Ortega, R., Perez, J.A.L., Nicklasson, P.J. and Sira-Ramirez, H.J. (2013). *Passivity-Based Control of Euler–Lagrange Systems: Mechanical, Electrical and Electromechanical Applications*, Springer, Berlin.

Qian, D. and Yi, J. (2016). *Hierarchical Sliding Mode Control for Under-Actuated Cranes*, Springer, Heidelberg.

Ramli, L., Mohamed, Z., Abdullahi, A.M., Jaafar, H. and Lazim, I.M. (2017). Control strategies for crane systems: A comprehensive review, *Mechanical Systems and Signal Processing* **95**: 1–23.

Saeidi, H., Naraghi, M. and Raie, A.A. (2013). A neural network self tuner based on input shapers behavior for anti sway system of gantry cranes, *Journal of Vibration and Control* **19**(13): 1936–1949.

Sano, S., Ouyang, H., Yamashita, H. and Uchiyama, N. (2011). LMI approach to robust control of rotary cranes under load sway frequency variance, *Journal of System Design and Dynamics* **5**(7): 1402–1417.

Sira-Ramirez, H. and Agrawal, S.K. (2004). *Differentially Flat Systems*, CRC Press, Boca Raton, FL.

Smoczek, J. (2013). Evolutionary optimization of interval mathematics-based design of a TSK fuzzy controller for anti-sway crane control, *International Journal of Applied Mathematics and Computer Science* **23**(4): 749–759, DOI: 10.2478/amcs-2013-0056.

Smoczek, J. (2015). Experimental verification of a GPC-LPV method with RLS and P1-TS fuzzy-based estimation for limiting the transient and residual vibration of a crane system, *Mechanical Systems and Signal Processing* **62**: 324–340.

Smoczek, J. and Szpytko, J. (2017). Particle swarm optimization-based multivariable generalized predictive control for an overhead crane, *IEEE/ASME Transactions on Mechatronics* **22**(1): 258–268.

Solis, C.U., Clempner, J.B. and Poznyak, A.S. (2016). Designing a terminal optimal control with an integral sliding mode component using a saddle point method approach: A Cartesian 3D-crane application, *Nonlinear Dynamics* **86**(2): 911–926.

Spathopoulos, M. and Fragopoulos, D. (2001). Control design of a crane for offshore lifting operations shore crane, *in* A. Isidori *et al.* (Eds.), *Nonlinear Control in the Year 2000*, Springer, London, pp. 469–486.

Spathopoulos, M. and Fragopoulos, D. (2004). Pendulation control of an offshore crane, *International Journal of Control* **77**(7): 654–670.

Suh, J.-H., Lee, J.-W., Lee, Y.-J. and Lee, K.-S. (2005). Anti-sway position control of an automated transfer crane based on neural network predictive PID controller, *Journal of Mechanical Science and Technology* **19**(2): 505–519.

Sun, N., Fang, Y. and Chen, H. (2014). Adaptive control of underactuated crane systems subject to bridge length limitation and parametric uncertainties, *33rd Chinese Control Conference (CCC), Nanjing, China*, pp. 3568–3573.

Sun, N., Fang, Y. and Chen, H. (2015a). Adaptive antiswing control for cranes in the presence of rail length constraints and uncertainties, *Nonlinear Dynamics* **81**(1–2): 41–51.

Sun, N., Fang, Y., Chen, H. and He, B. (2015b). Adaptive nonlinear crane control with load hoisting/lowering and unknown parameters: Design and experiments, *IEEE/ASME Transactions on Mechatronics* **20**(5): 2107–2119.

Sun, N., Fang, Y., Chen, H., Lu, B. and Fu, Y. (2016). Slew/translation positioning and swing suppression for 4-DOF tower cranes with parametric uncertainties: Design and hardware experimentation, *IEEE Transactions on Industrial Electronics* **63**(10): 6407–6418.

Tar, J.K., Rudas, I.J., Bitó, J.F., Machado, J.A.T. and Kozłowski, K.R. (2010). Adaptive tackling of the swinging problem for a 2 DOF crane–payload system, *in* I.J. Rudas *et al.* (Eds), *Computational Intelligence in Engineering*, Springer, Berlin/Heidelberg, pp. 103–114.

Vazquez, C., Fridman, L. and Collado, J. (2012). Second order sliding mode control of a 3-dimensional overhead-crane, *51st Annual Conference on Decision and Control (CDC), Maui, HI, USA*, pp. 6472–6476.

Vázquez, C., Fridman, L., Collado, J. and Castillo, I. (2015). Second-order sliding mode control of a perturbed-crane, *Journal of Dynamic Systems, Measurement, and Control* **137**(8): 081010.

Vukov, M., Van Loock, W., Houska, B., Ferreau, H.J., Swevers, J. and Diehl, M. (2012). Experimental validation of nonlinear MPC on an overhead crane using automatic code generation, *American Control Conference (ACC), Montréal, Canada*, pp. 6264–6269.

Wu, Z., Xia, X. and Zhu, B. (2015). Model predictive control for improving operational efficiency of overhead cranes, *Nonlinear Dynamics* **79**(4): 2639–2657.

Yang, J.H. and Shen, S.H. (2011). Novel approach for adaptive tracking control of a 3-d overhead crane system, *Journal of Intelligent & Robotic Systems* **62**(1): 59–80.

Yu, W., Li, X. and Panuncio, F. (2014). Stable neural PID anti-swing control for an overhead crane, *Intelligent Automation & Soft Computing* **20**(2): 145–158.

Zheng, Q. and Gao, Z. (2010). On practical applications of active disturbance rejection control, *29th Chinese Control Conference, Beijing, China*, pp. 6095–6100.

Carlos Aguilar-Ibanez obtained his BSc in physics in 1990 at the Higher School of Physics and Mathematics of National Polytechnic Institute (IPN), Mexico City. From the Center for Research and Advanced Studies (CINVESTAV) of IPN he received the MSc degree in electrical engineering in 1994, and the PhD degree in automatic control in 1999. Since then he has been a researcher in the Computer Research Center of IPN. His research focuses on non-linear systems, systems identification, observers, automatic control, and chaos theory.

Miguel S. Suarez-Castanon was born in 1967. He received the BEng degree in cybernetics and computer science from the School of Engineering of the University of Lasalle in 1989. From the Research Institute of Applied Mathematics and Systems of the National Autonomous University of Mexico he received the MSc degree in computer science in 2001. In 2005 he received the PhD degree in computer science at the computer research center of the National Polytechnic Institute of Mexico.

Appendix

Convergence analysis

Properties of the Bézier function. Note that

$$\dot{\lambda}(t,t_i,t_f) = -1260\frac{(t-t_i)^4(t-t_f)^5}{\delta_T^{10}}, \tag{A1}$$

$$\ddot{\lambda}(t,t_i,t_f) = -1260\frac{(t-t_i)^3(9t-5t_i-4t_f)(t-t_f)^4}{\delta_T^{10}}. \tag{A2}$$

Evidently, B1 is fulfilled. If we iteratively derive (A1) and (A2), B1 always holds. From (A1) and (A2), we prove that B2 also holds. That is, from (A2) we conclude that either the maximum or the minimum of $\dot{\lambda}$ is given by

$$9t - 5t_i - 4t_f = 0,$$

leading to

$$t_1 = \frac{5t_i + 4t_f}{9}. \tag{A3}$$

Now, substituting (A3) into (A1), we obtain

$$\dot{\lambda}(t_1,t_i,t_f) = \frac{112000000}{43046721\delta_T} \approx \frac{2.61}{\delta_T}.$$

Similarly, it is easy to see that $\dddot{\lambda}(t,t_i,t_f) = 0$ implies that the maximum or the minimum are located at

$$t_2 = \frac{10t_i + (t_i+t_f)\sqrt{10}5t_i + 8t_f}{18}.$$

Substituting the above values of t_2 into (A2), we get

$$\ddot{\lambda}(t_2,t_i,t_f) = \frac{8\left(1415 + 8048\sqrt{10}\right)}{\delta_T^2} \approx \frac{11.01}{\delta_T^2}.$$

To prove property B3, we must note that $\dot{\lambda}(t,t_i,t_f) \geq 0$ for all $t \in (t_i,t_f)$. Therefore, we have

$$\int_0^\infty \dot{\lambda}^2(s,t_i,t_f)\,\mathrm{d}s \leq \frac{\kappa_1}{\delta_T}\int_{t_i}^{t_f} \dot{\lambda}(s,t_i,t_f)\,\mathrm{d}s = \frac{\kappa_1}{\delta_T} \leq \infty,$$

implying that $\dot{\lambda}(t,t_i,t_f) \in L_2^2$. In a similar fashion, we can show that $\ddot{\lambda}(t,t_i,t_f) \in L_2^2$. Notice that $\dot{x}_d(t) = (x_f - x_i)\dot{\lambda}(t,t_i,t_f)$ and $\dot{y}_d(t) = (x_f - x_i)\dot{\lambda}(t,t_i,t_f)$ (see (3)). Accordingly, we can conclude that $\dot{x}_d(t)$, $\dot{y}_d(t)$ $\in L_2^2$. Evidently, $\ddot{x}_d(t)$, $\ddot{y}_d(t) \in L_2^2$ also holds.

Received: 13 December 2018
Revised: 29 May 2019
Accepted: 10 August 2019